

Nanopatterning by block copolymer micelle nanolithography and bioinspired applications

Theobald Lohmüller,^{a),b)} Daniel Aydin,^{b)} Marco Schwieder, Christoph Morhard, Iliia Louban, Claudia Pacholski, and Joachim P. Spatz^{c)}

Department of New Materials and Biosystems, Max Planck Institute for Metals Research, Heisenbergstrasse 3, 70569 Stuttgart and Department of Biophysical Chemistry, University of Heidelberg, INF253, 69120 Heidelberg, Germany

(Received 27 October 2010; accepted 21 December 2010; published 16 February 2011)

This comprehensive overview of block copolymer micelle nanolithography (BCM_N) will discuss the synthesis of inorganic nanoparticle arrays by means of micellar diblock copolymer approach and the resulting experimental control of individual structural parameters of the nanopattern, e.g., particle density and particle size. Furthermore, the authors will present a combinational approach of BCM_N with conventional fabrication methods, namely, photolithography and electron beam lithography, which combines the advantages of high-resolution micronanopatterning with fast sample processing rates. In addition, the authors will demonstrate how these nanoparticle assemblies can be transferred to polymer substrates with a wide range of elasticity. In the second part of this report the authors will introduce some of the most intriguing applications of BCM_N in biology and materials science: The authors will demonstrate how nanoparticle arrays may be used as anchor points to pattern functional proteins with single molecule resolution for studying cellular adhesion and present a technological roadmap to high-performance nanomaterials by highlighting recent applications for biomimetic optics and nanowires. © 2011 American Vacuum Society. [DOI: 10.1116/1.3536839]

I. INTRODUCTION

Nanomaterials show remarkable physical and chemical properties due to their small size. In 1959, Feynman was the first to foresee the evolution of nanoscience and nanotechnology into a broad interdisciplinary research field with important applications in industry when he spoke about “the problem of manipulating and controlling things on a small scale.”^{1–4} The synthesis of nanosized objects in predefined patterns remains a challenge and there is ongoing demand for innovative fabrication methods to generate nanoscale materials and devices. As a general rule, two strategies for nanofabrication can be identified: “top down” and “bottom up.”

Top-down strategies encompass methods such as photolithography,^{5,6} x-ray lithography,^{7,8} electron beam (e-beam),⁹ and focused ion beam (FIB) (Refs. 10 and 11) lithography. Photolithography and optical lithography are the two most widely used conventional nanofabrication technologies in the semiconductor industry due to their high throughput in sample processing.¹² However, as they use light, the method is theoretically diffraction limited and structural dimensions below 100 nm are hardly accessible. Cutting-edge interference and immersion methods employ deep and extreme ultraviolet lasers as a radiation source to obtain sub-30-nm resolution.¹³ Similar to e-beam and FIB lithography a photomask is not needed in this case. However,

all of these methods require highly specialized expensive technical equipment and the sample processing rates are limited by the scanning speed.

Bottom-up strategies use the self-organization of molecules to generate structured materials without external intervention.¹⁴ Throughout nature, self-assembly is the dominating fabrication concept for inorganic and biological systems.^{15–17} In materials science and nanofabrication, self-assembly based methods are particularly attractive as they are generally inexpensive and widely applicable and can even reach subnanometer resolution.^{18,19} Two types of self-assembly can be distinguished: dynamic and static.¹⁷ Dynamic systems such as biological cells possess the ability to link the dissipation of energy to processes that create molecular order in the cell, i.e., pattern formation. As a result they are able to reorganize themselves autonomously in response to their environment. Static systems, such as molecular crystals, self-organize into structures which represent the minimum of their free energy or are kinetically trapped in an intermediate energy state and therefore remain stable, a prerequisite for manufacturing. Several methods and strategies have been developed to utilize static self-assembly for nanoscience and technology. Examples include self-assembled monolayers,^{18,20} block copolymer lithography,^{21–24} and colloidal lithography.^{25,26} In most of these self-assembled systems, extended and periodic structures are formed from individual building blocks such as molecules and particles, which also set their characteristic length scale. Spatial control and guided organization of individual nanometer-sized objects into aperiodic morphologies, however, is extremely challenging.^{18,27–29} One way of creating aperiodic morpholo-

^{a)}These authors contributed equally to this work.

^{b)}Present addresses: Materials Sciences Division, Lawrence Berkeley National Laboratory, Berkeley, CA 94720 and Department of Chemistry, University of California, Berkeley, CA 94720.

^{c)}Electronic mail: spat@mf.mpg.de

TABLE I. BCMN: Methods and applications.

	References
Nanoparticle synthesis and nanopatterning	
Particle spacing	41 and 42
Particle size	43–45
Micronanopatterning	46, 42, and 47–50
Nanostructured flexible materials	51 and 52
Biological applications of BCMN	
Biofunctionalization of nanoparticles	50 and 53
Cell studies	41 and 54–64
Materials science applications for BCMN	
Antireflective interfaces	65
Photonic materials	66
Growth of inorganic/organic nanowires	46, 67–69, and 149

gies is through chemical or topographical manipulation of the substrate prior to patterning. This enables a selective organization into predefined templates by either van der Waals, ionic interactions, or covalent binding.^{30,31} Furthermore, it is possible to deposit molecules directly using lithographic methods such as microcontact printing (μ CP) (Refs. 32–34) or dip-pen nanolithography (DPN).^{35,36} There molecular building blocks are used as “ink” which is layered (DPN) or stamped (μ CP) from a conventionally fabricated master onto selected areas on a solid substrate. Hereafter, these self-assembled materials can be used directly as a lithographic resist for further modification and processing. Examples include scanning probe lithography based technologies such as nanografting,^{37,38} near-field scanning optical lithography,³⁹ and nanoimprint lithography.⁴⁰ As these three examples show, the combination of bottom-up strategies with conventional top-down technology is the key to successful user-defined nanopatterning.

In this overview we want to present nanolithography with diblock copolymer micelles as an intriguing bottom-up approach for high-throughput nanoparticle synthesis in well-aligned and organized patterns and demonstrate their applicability for the fabrication of nanostructured functional materials and devices. We start with the experimental aspects that account for the great versatility of this approach in nanoresearch, followed by a discussion of some of the most recent applications for biology and materials science. A comprehensive list of publications with detailed information is given in Table I.

II. BLOCK COPOLYMER MICELLE NANOLITHOGRAPHY

Block copolymer nanolithography⁷⁰ and in particular block copolymer micelle nanolithography (BCMN) (Refs. 71 and 72) are fascinating methods for nanopatterning in a size range below 100 nm, a range that is hardly accessible by technically less sophisticated standard lithographic techniques. BCMN is based on the spontaneous formation of

microphase-separated morphologies from amphiphilic block copolymers and the long-range alignment of the newly created subunits into extended nanopatterns.⁷³

Block copolymers are compounds consisting of blocks of different monomers. In the case of polystyrene(*x*)-*block*-poly(2-vinylpyridine)(*y*) [PS(*x*)-*b*-P2VP(*y*)], one molecule contains two polymer blocks, PS and P2VP, which are linked by a covalent bond at their respective ends. When dissolved in toluene the polymer molecules are present in form of single chains. Above a certain concentration, the “critical micelle concentration” (CMC), the molecules start to organize themselves into spherical micelles while the number of individual free chains in solution remains constant.^{74–76} Since toluene is a solvent highly selective to polystyrene, micellation takes place: the PS block forms the outer micellar shell whereas the less soluble P2VP block forms the core.⁷⁷ This core-shell configuration represents a nanoreactor that enables the selective dissolution of metal precursor salts into every micelle.^{78,79} The loading rate of the micelles is defined by the stoichiometric ratio of metal salt versus the number of vinyl pyridine units. In equilibrium the distribution of the precursor in the micelles varies only marginally between the micelles.⁸⁰ Both the thermodynamic properties of the micellar solution and the kinetic stability of the micelles are affected by the incorporation of metal ions into the micellar core. Adding metal salt to a PS-*b*-P2VP micellar solution in toluene causes ionic interactions between the metal salt and P2VP chains, which, in turn, decreases the CMC significantly due to an increased incompatibility between the solvent and the P2VP/metal salt complex. As a consequence the micellar structure is kinetically trapped and micelles dissociate very slowly.^{79,81} A schematic depiction of the micellization process of diblock copolymers is shown in Fig. 1(a).

A micellar monolayer can be formed by either spin or dip coating a substrate. Dip coating has the advantage of fast and uniform decoration of plain and curved substrates with high accuracy regardless of substrate size. During sample retraction, the micelles are organized into a quasihexagonal monolayer on the substrate surface [Figs. 2(a)–2(f)]. The driving force for this assembly process is the emerging capillary force during solvent evaporation at the immersion edge [Fig. 1(b)]. The lateral order of the micelles is a result of the balance between attractive capillary forces and repulsive electrostatic and steric interactions. Afterward, the polymer matrix is removed by exposing the sample to hydrogen or oxygen plasma, which leaves only metal or metal oxide clusters on the surface [Figs. 2(e)–2(h)].⁸² Side view transmission electron microscopy images revealed that the particles are nearly spherical in shape [Fig. 2(j)].⁷² Various particle compositions such as pure metal clusters (Au, Ag, Pd, Pt, Co, and Ni),^{43,46,72,82} metal alloys such as FePt,^{83,84} and oxides (TiO₂, Fe₂O₃, and ZnO) (Ref. 84) have been generated using the respective precursor salt. Noble metal nanoparticles are of special interest for various applications⁸⁵ due to their particle size and shape at the nanoscale, which is reflected in

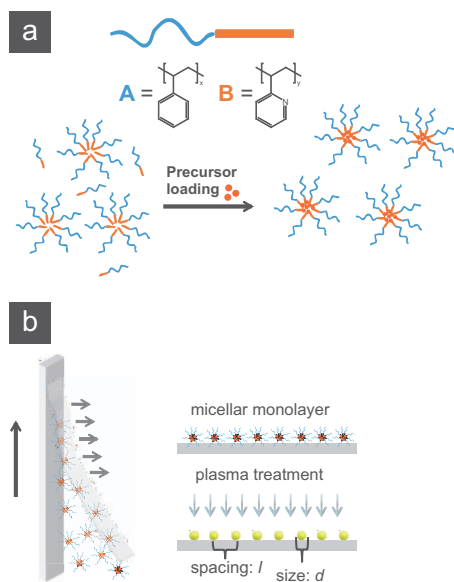


FIG. 1. (Color) Schematic illustration of the concept of block copolymer micelle nanolithography: (a) poly(styrene)-*block*-poly(2-vinylpyridine) (PS-*b*-P2VP) diblock copolymers are dissolved in toluene. By adding a metal salt precursor to the solution, metal ions diffuse into the micellar core leading to an equally distributed amount of precursor inside each micelle. (b) An extended monolayer of micelles is formed on top of a solid substrate by dip coating. The polymer is then removed by a subsequent plasma treatment of the substrate, reducing the precursor salt into hexagonally aligned individual metal nanoparticles.

their unique and superior optical,^{86–89} electronic,^{90,91} and catalytic^{92,93} properties compared to bulk metals.

The two biggest advantages of micelle nanolithography are its applicability to a wide range of different substrate materials and shapes and the significant mechanical stability of the deposited nanoparticles on the substrate in comparison to other nanoparticle deposition methods (e.g., pure evaporation-based processes). The choice of substrate material is influenced by two important material properties. Most importantly it must be persistent against solvent and plasma processing. Different substrates such as glass, silicon, diamond, sapphire, SrTiO₃, and mica have been used successfully for BCMN.^{72,82} The second crucial property is the me-

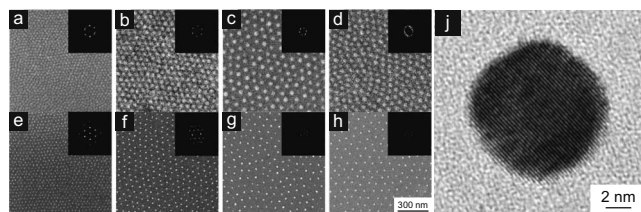


FIG. 2. Particle spacing can be controlled on the nanometer scale by using diblock copolymers with different molecular weight. Top row (a)–(d): SE micrographs of micellar monolayers prior to plasma treatment. Bottom row (e)–(h): SE micrographs of Au nanoparticle arrays after removal of the polymer shell and reduction of the precursor salt to elemental gold by hydrogen plasma treatment. (j) TE micrograph of gold nanoparticle synthesized by BCMN (a)–(h) modified from Ref. 41. The inset of (a)–(h) shows Fourier analysis pattern data of the respective image indicating the order of the nanoparticle pattern.

chanical stability of the nanoparticles on the substrate. It is a highly desired feature of nanoparticle arrays that the nanoparticles neither diffuse laterally on the surface nor coalesce to larger particles at high temperatures. While nanoparticles stick very well to mica, glass, GaAs, Si wafer, or SiO_x wafer, they stick less firmly to SrTiO₃. The cause for higher stability on some surfaces is the modification of the interface between nanoparticle and substrate by the plasma process. Gold nanoparticles, for example, get partly embedded into glass or SiO_x layers on Si wafers during the plasma process, giving the nanoparticle its superb mechanical stability.

BCMN is a straightforward approach to nanoparticle fabrication and patterning but when it comes to functional applications, precise control over structural parameters (namely, particle spacing and size) is crucial. The size, shape, and spacing of noble metal particles, for example, determine their optical properties.^{94–97} When studying biological systems, the precise location of nanoparticles on interfaces also plays a crucial role.^{41,54–59,98}

In Sec. II A we will discuss in detail the experimental factors that influence interparticle spacing and particle size and demonstrate how both parameters can be controlled independently of each other.

A. Control of nanoparticle spacing

From an experimental viewpoint several parameters that influence the spatial distribution of nanoparticles due to block copolymer micelle self-assembly can be varied: (i) the micellar size, (ii) the amount of metal precursor that is loaded into the micelles, (iii) the concentration of the polymer solution,⁹⁹ and (iv) the retraction speed of the substrate from the micellar solution.^{54,100,101}

The micellar size can be controlled by increasing the polymer length, the amount of metal precursor per micelle,^{42,71} and by adding small amounts of water, which then diffuse into the polar micellar core. Because a greater volume fraction of incorporated metal ions leads to stronger interactions between the ionized PVP block and the nonpolar solvent, the size of the micelles increases as well, resulting in a lower packing density when the micelles are transferred to the substrate.⁷⁹ Modifying the metal salt concentration in the polymer solution also influences the size of the resulting nanoparticles. Nonetheless, varying the amount of metal salt in the solution has only marginal influence on particle spacing and allows little variability. Changing the molecular weight of the diblock copolymer to form larger micelles¹⁰² is another approach to control interparticle spacing (Fig. 2). The disadvantage of varying the polymer length is that it is time consuming to adjust particles made from different polymers to be identical in size. This requires optimizing the loading rate for every polymer and every desired spacing distance.

How to achieve the greatest variability with a minimum of time and effort? Two approaches have proven to be successful: changing the concentration of the copolymer in the micellar solution when working with a single diblock copolymer (Fig. 3) (Ref. 103) or varying the speed at which the

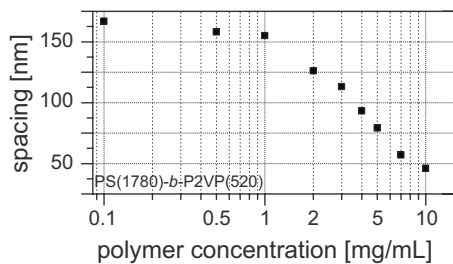


FIG. 3. Particle spacing as a function of the polymer concentration exemplified for PS(1780)-*b*-P2VP(520).

substrate is retracted from the micellar solution during coating. By modifying the retraction velocity we were able to produce continuous gradients of particle spacings between 60 and 250 nm using only four different micelle solutions (see Fig. 4). In all our experiments an increase in retraction velocity yielded tighter spacing between nanoparticles after plasma treatment. As reported by Darhuber *et al.*,¹⁰⁴ two parameters influence the thickness of a film deposited on a substrate by dip coating perpendicular to a fluid interface: the retraction velocity at which the sample is withdrawn from the solution and the viscosity of the solution. This coincides with our observations that adding more polymer to the toluene solution, thus increasing its viscosity, correspondingly results in a tighter particle density.

B. Controlling the particle size

The particle size is restricted by the amount of metal salt that can be incorporated into the micellar core and thus di-

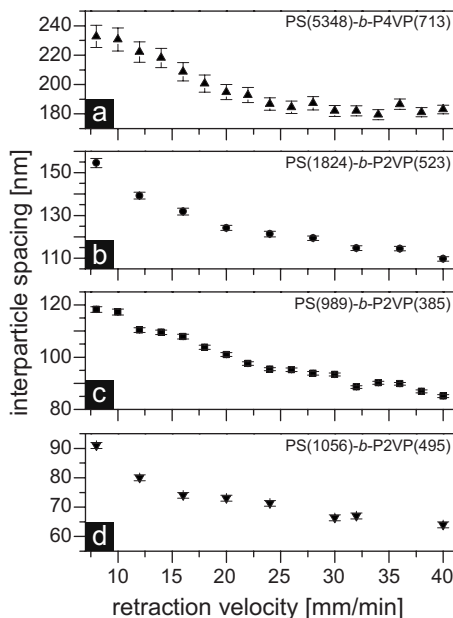


FIG. 4. Particle spacing as a function of the retraction velocity. The spacing between the nanoparticles is altered depending on the speed at which the substrate is pulled out of the micellar solution during coating. Using the same polymer solution, the difference in interparticle spacing of gold clusters can be varied up to 40 nm simply by alternating the retraction velocity, thus allowing the production of spacing gradients.

rectly correlates with the molecular weight of the PVP block. Particle diameters range from approximately 1 to 12 nm. To obtain larger diameters it is necessary to implement an additional growing or postloading step, which allows for the enlargement of the established surface-confined metal particles. Electroless deposition by hydroxylamine seeding provides a method for the selective enlargement of colloidal Au particles in solution and on substrates.^{105,106} During hydroxylamine seeding, the existing Au metal particles act as catalytic nuclei for the electroless deposition of metal ions from the surrounding solution using hydroxylamine (NH₂OH) as the reducing agent. Since the reduction of metal ions on the surface of deposited nanoparticles is kinetically more favorable than the reduction rate for metal ions in solution, the nucleation of new particles is prevented and metal ions add to the growth of existing nanoparticles.¹⁰⁷ As a result the nanoparticles turn out to be similar in size.

The difficulty of using hydroxylamine seeding for particle enlargement lies in preventing surface-confined metal particles from parting from the surface into the solution. Because the nanoparticles are not covalently bound to the substrate, it is important to stabilize them before additional growth. Otherwise detaching nanoparticles can destroy the spatial geometry of the nanopattern. Stabilization can be achieved either by embedding the nanoparticles into a matrix of alkyl siloxane molecules or by using the diblock copolymer matrix directly as a stabilizing template.⁴³ The gold particles, although they are embedded into the matrix, are not fully covered by it, allowing subsequent hydroxylamine seeding. For example, when using 7 nm particles the height of the surrounding layer corresponds to approximately one-third of the particle diameter. By varying the type of metal used for seeding and the interparticle distance, the precise preparation of highly ordered monometallic and bimetallic core-shell nanostructures is possible.⁴⁴ However, depending on the surface chemistry of the monolayer matrix, embedding the particles can be difficult and undesirable. In comparison, using the polymer shell of the micelles themselves as a stabilizing template offers a fast and substrate independent approach. During the initial phase of plasma treatment the outermost parts of the polymer matrix are etched off without disturbing the polymer film on the substrate. It is during these first few minutes of plasma treatment that the metal particles in the micelles become exposed and elemental particles are formed, which are needed as seeds for the following hydroxylamine reduction.⁸² This intramicellar approach represents a fast and substrate independent procedure that offers a very broad applicability. Scanning electron (SE) micrographs for Au, Pt, and Pd particle arrays before (upper panel) and after (lower panel) electroless deposition are shown in Fig. 5.

C. Micronanopatterning

The ambition to optimize the production of nanopatterned surfaces has led to combining BCMN, a bottom-up approach, with conventional top-down technology. As a result it has become possible to generate any desired particle con-

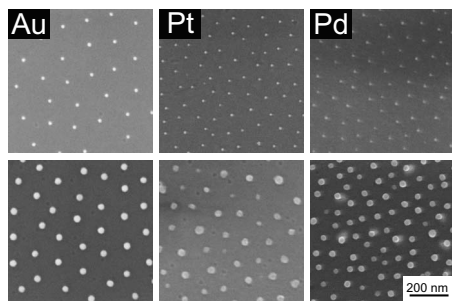


FIG. 5. Au, Pt, and Pd particles grown by intramicellar electroless deposition. SE micrographs of Au, Pt, and Pd particles on glass cover slips before (top; 7 nm initial size) and after (bottom; 25 nm) particle growth. Adapted from Ref. 43.

figuration, ranging from micron-sized nanopatterned corals down to a single particle (Fig. 6).¹⁰⁸ As an additional advantage the number of particles on the surface can be adjusted independent of interparticle spacing.

The top-down methods that have been used in combination with BCMN are listed in Table II and three of them are depicted in Fig. 6. The techniques published thus far can be divided into two groups, those using serial processes and those working with parallel process technology. The first group, which includes most top-down methods, involves direct modification of the micelles by localized irradiation with UV light,⁴⁷ electrons,⁴² or ions.⁴⁸ Speaking in favor of these methods is their high resolution with respect to feature size but at the same time the limited overall surface area that can be patterned in a reasonable amount of time poses a significant limitation. One example that uses serial processes is e-beam lithography, which allows for the patterning of user-

defined arrays of individual nanoparticles on conductive as well as nonconductive substrates by pinning down single micelles with an electron beam [Fig. 6(a)].^{42,46} On the downside, only a few square millimeters can be patterned over the course of several hours. Parallel process technology, in comparison, allows much faster sample processing but thus far has failed to achieve feature sizes in the submicron range. Examples for parallel processes include the deposition of micelles into prestructured cavities and microcontact printing of micelles.^{109,110} While standard microcontact printing can lead to the formation of multilayers with a random particle order at the edges of the stamp, this can be avoided by using a microcontact deprinting approach as reported by Chen *et al.* [Fig. 6(b)].⁴⁹ Nevertheless, it can be said that there is no “one size fits all” solution for producing a desired nanopattern using these approaches and more often than not a compromise between feature size and processing rate has been the determining factor when deciding which is the method of choice.

To address this predicament we recently developed an approach for the fabrication of square centimeter-sized surface areas of nanostructured microcorals by using photolithography and e-beam lithography on a photoresist applied to the nanoparticle array. By using a resist, instead of irradiating the micellar film directly, we were able to expedite the processing rate over 200 times compared to previous methods with submicron resolution [Fig. 6(c)].⁵⁰ The considerably improved turnover rates are particularly relevant for biological screening applications, where high sample throughput is essential.

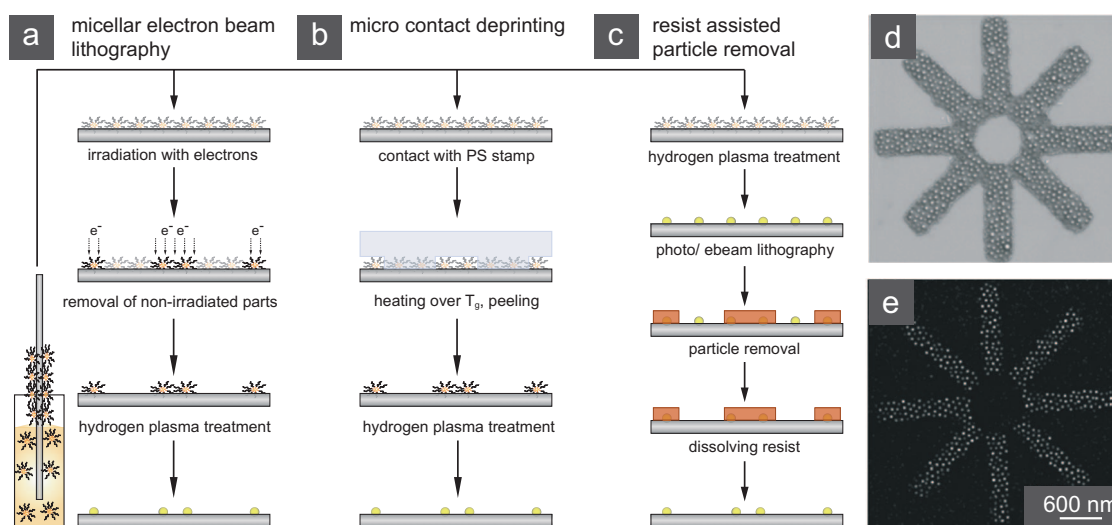


FIG. 6. (Color) Micronanopatterning. (a) Micellar electron beam lithography: user-defined patterns can be written into a micellar monolayer with an electron beam, followed by the removal of nonirradiated micelles. Subsequent hydrogen plasma treatment leads to the respective micronanostructured gold particles. (b) Microcontact deprinting: a topographically micropatterned PS stamp is placed on a micellar monolayer and the assembly is heated above the glass transition temperature (T_g) of PS. Those micelles that were in contact with the protrusions of the stamp can then be removed by peeling off the stamp. The following plasma process generates the desired nanoparticle pattern. (c) Resist-assisted particle removal: extended arrays of gold nanoparticles are covered with a strippable resist, which is then structured by means of photo or electron beam lithography. After removal of the particles in unprotected regions, the resist is dissolved and uncovers the micronanostructure. (d) Star-shaped micronanostructure fabricated by micellar electron beam lithography before and after (e) plasma treatment. (d) and (e) are reproduced from Ref. 71.

TABLE II. Processes for fabrication of micronanostructures.

Method	Feature size	Process speed	Reference
Electron beam irradiation onmicellar monolayer	<100 nm	<0.1 mm ² /h	46 and 42
Focused ion beam irradiation onmicellar monolayer	<100 nm	<10 mm ² /h	48
UV irradiation on micellar monolayer	>10 μm	Parallel	47
Microcontact printing of micellar solution	2 μm	Parallel	109
Microcontact deprinting of micellar monolayer	1 μm	Parallel	49
UV resist lithography with particle removal	3 μm	Parallel	50
E-beam resist lithography with particle removal	100 nm	<3 mm ² /h	50

D. Nanoparticle transfer to flexible nonconductive substrates

Hydrogels of water soluble, nontoxic, and protein-repellent poly(ethylene glycol)-diacrylate (PEG-DA) macromolecules are of particular interest for biological applications due to their exceptional material properties. Defined by Young's modulus (E_Y), a measure of the stiffness of an isotropic elastic material, hydrogels are characterized by their adjustable stiffness. The two parameters that determine the tensility of the hydrogel are the molecular weight of the PEG-DA molecule and the water content (C_{H_2O}) of the aqueous PEG-DA solution prior to polymerization. The stiffness of the gels can be adjusted within four orders of magnitude [$0.6 \text{ kPa} \leq E_Y(M_W, C_{H_2O}) \leq 6 \text{ MPa}$], covering the elasticity of all tissues found in the human body (Fig. 7).⁵¹

BCMN is a method that is limited to inorganic supports and is not suitable for flexible polymer-based materials. Polymers, such as polystyrene (PS), polydimethylsiloxane (PDMS), or PEG-DA, are either dissolved by the micelle solution, degraded by plasma treatment, or both. To circumvent this limitation we have developed a technique that enables the transfer of nanoparticles from rigid supports such as glass or silicon to flexible polymeric substrates.⁵² In a first step, unsaturated transfer linker molecules are covalently bound to the nanoparticles on the rigid substrate. Then, the supported nanoparticles are covered with a polymer cast.

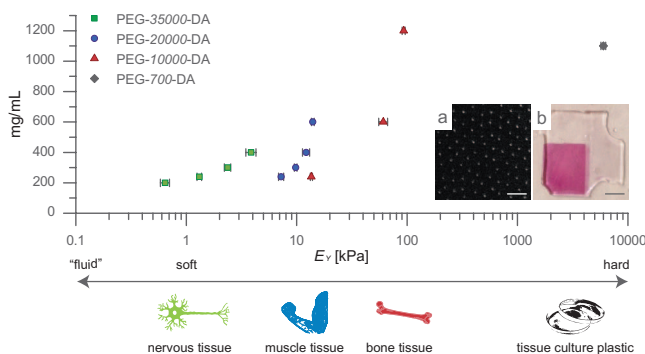


FIG. 7. (Color) Young's moduli (E_Y) of PEG-DA hydrogels polymerized with different initial water contents could be varied over four orders of magnitude from glassy PEG-700-DA (6 MPa) to gelatinous PEG-35000-DA (0.6 kPa). Inset: (a) cryo scanning electron micrograph of PEG-20000-DA surface after Au nanoparticle transfer procedure. Scale bar 100 nm. (b) Plasmon absorbance of Au nanoparticles on PEG-DA hydrogels after growth by electroless deposition. Here: extended nanostructures on PEG-700-DA sample. Adapted from Ref. 51.

Linkers functionalized with PEG hydrogel diacrylate (DA) are immobilized onto the gold nanoparticle surface and then covered with PEG-DA. Subsequent UV radiation of the polymer cast results in cross-linking of the PEG-DA and the nanoparticle immobilized linker within the PEG-DA cast. In the case of hydrophobic polymers such as PS and PDMS, 2-propene-1-thiol is used as a transfer linker. Afterward, the polymer cast is cured by solvent evaporation or cross-linking through exposure to high temperatures. During this step the linker molecules form a connection between the gold particles and the solidified polymer. Finally, the inorganic support is removed by mechanical peeling or chemical etching [Fig. 8(c)].

The right choice of linker is crucial for efficient particle transfer in this experiment. Without effective linkage nanometer-sized pores are generated on top of the polymer surface corresponding to the negative cast of the nanoparticle template [Fig. 8(d)]. Using this strategy, we were able to transfer nanoparticles to PEG-DA hydrogels independent of the hydrogel's mechanical properties.

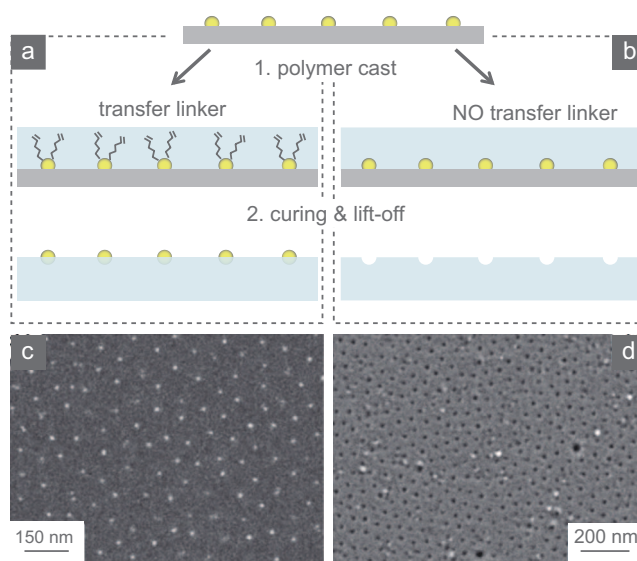


FIG. 8. (Color) (a) Gold nanoparticles can be transferred to polymeric materials using an appropriate transfer linker. The linker is covalently bound to the particles and cross-linked into the polymer cast. After curing and lift-off, the particles are completely transferred into the polymer surface. (b) In absence of linker molecules a porous imprint is generated. (c) and (d) SE micrographs of PDMS (c) with and (d) without gold particles. Adapted from Ref. 52.

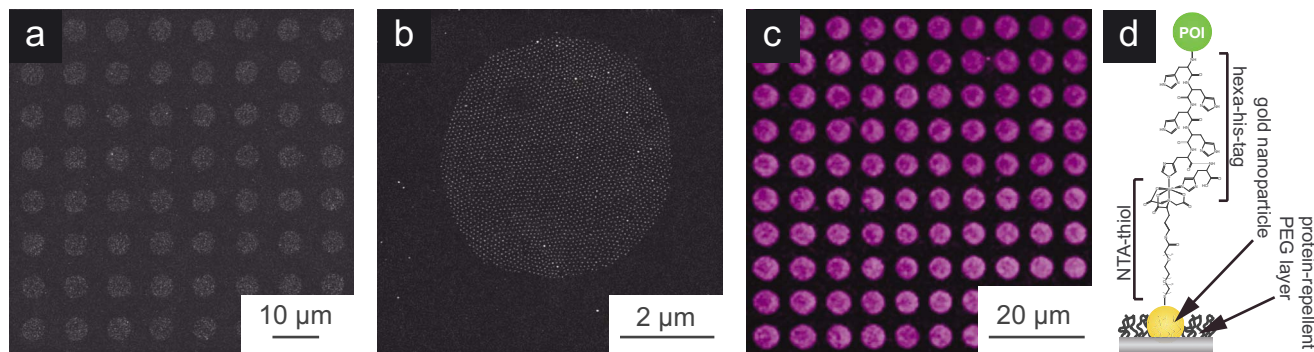


FIG. 9. (Color online) Gold nanoparticle arrays can be selectively decorated with histidine-tagged proteins. The interparticle areas of micronanostructured surfaces (a) and (b) are passivated with protein-repellent poly(ethylene glycol) while the gold nanoparticles are functionalized with NTA-thiol and loaded with Ni^{2+} . The NTA-Ni complex now functions as an acceptor for histidine-tagged proteins. (c) A fluorescence micrograph of dye-conjugated antibodies immobilized via histidine-tagged protein A. (d) Illustration depicting the immobilization chemistry.

These results represent an important advancement of BCMN with a great perspective for future applications in cell biology and tissue engineering.^{60,111}

III. NANOPARTICLE APPLICATIONS

A. Nanoparticle interfaces in biology

The awareness that biological life takes place on a molecular level and recent advances in nanoscale research have opened the door for many new developments in the field of molecular life sciences. The ability to produce a wide variety of biologically active materials to influence cell behavior at the nanoscale^{60,111–113} has fueled interest in nanobiotechnology applications ranging from biosensors,¹¹⁴ protein arrays,¹¹⁵ and molecular motors¹¹⁶ to engineered nanopores,¹¹⁷ nanotubes,¹¹⁸ and computing.¹¹⁹

In all these applications biological compounds are functionalized to a solid nanopatterned surface by covalent linkage. However, because the functional properties of proteins and DNA depend on their orientation,¹²⁰ maintaining the biological activity of surface-immobilized biomolecules poses a great difficulty. Gold nanoparticle arrays have proven to be particularly suitable as a platform for site-directed functionalization of biomolecules.^{50,53,121} One example is the selective coupling of histidine-tagged proteins L1, agrin, and N-cadherin to gold nanoparticles using a mono-NTA-thiol linker system by Wolfram *et al.* (Fig. 9).⁵³ Unspecific protein adsorption to the glass substrate was avoided by a covalent¹²² or electrostatically¹²³ bound monolayer of poly(ethylene glycol) between the particles. This technique is widely applicable for the display of his-tagged proteins in a site-specific manner on a substrate with predefined lateral spacing and an evenly distributed high concentration of active molecules.

Cell adhesion research is one area where extensive studies with peptide-functionalized substrates have been conducted. The key player in mediating cell adhesion to the surrounding extracellular matrix (ECM) is a certain class of transmembrane receptors, the so-called integrin family.¹²⁴ A prominent recognition sequence for integrins found in many ECM components is a peptidic sequence consisting of three amino ac-

ids: arginine, glycine, and aspartic acid (RGD: arginine-glycine-aspartic acid).¹²⁵ Several groups have shown that the density and lateral distribution of cell-adhesive ligands are crucial for cell adhesion and survival.^{126–128} For investigating in greater detail the molecular interactions between cells and the ECM, such as the number of receptor-ligand interactions necessary for cell survival or the spatial constraints of the ligand, the application of user-defined nanopatterns presents a very promising approach. BCMN enabled the investigation of the molecular interaction of individual transmembrane proteins with biofunctionalized gold particles, which led to striking new insights into the cooperation of transmembrane proteins. These experiments showed that cell adhesion was impaired above a certain spacing threshold. The ability of several cell types to adhere to substrates with RGD-functionalized gold nanoparticles decreased dramatically above separation distances of 58 nm (Fig. 10).⁴¹ Based on the following three observations, the effect was attributed to the necessity of $\alpha_v\beta_3$ integrin clustering for proper focal contact formation:^{56,57,61,129} The reduced number of adhering cells, a decrease in the cell spreading area, and a reduced adhesion force on nanoparticles spaced greater than 58 nm apart.^{58,59,98} This has led to the use of spacing gradients to study how cells are able to sense spatial variations of single binding sites for adhesion receptors and the consequences on cell polarization and migration.^{54,62} Investigating the dynamic response of MC3T3 osteoblasts on an RGD-nanoparticle gradient revealed that a minimal special difference of 15 nm/mm is required for cells to polarize on particle pattern with separation distances ranging from 50 to 80 nm along the substrate. The osteoblasts polarized toward a higher density of adhesion ligands while their morphology changed between radial (for a ligand spacing of ≥ 50 nm) to strongly elongated (for a spacing of ≤ 80 nm). These experiments provide evidence for the ability of cells to sense spatial variations of single adhesion binding sites presented by the artificial extracellular environment with single nanometer accuracy across the cell. Nanopatterned interfaces are also a powerful method to mimic cell-cell contacts. One example is the regulation of neuron attachment and neurite outgrowth from the immunoglobulin superfamily member DM-GRASP

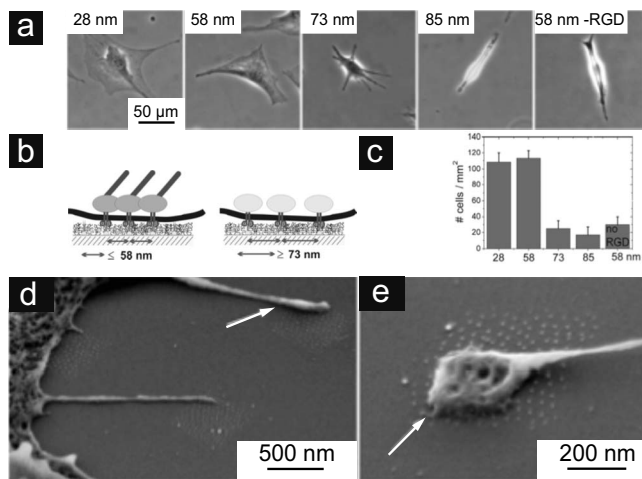


FIG. 10. Cell adhesion mediated by $\alpha_5\beta_3$ integrin is dependent on the spacing of cRGDFK functionalized gold nanoparticles. (a) Cell spreading is impaired on substrates with interparticle distances greater than 58 nm. (b) On the molecular level this effect is attributed to the fact that integrins must be in close proximity to each other for cluster formation. (c) The number of viable cells on a given substrate decreases when a threshold spacing of 58 nm is exceeded. (d) and (e) Cells attach and align to micronanostructures which promote cell adhesion when particles are spaced apart 58 nm or less. Adapted from Ref. 41.

presented on a nanopattern (GRASP: ‘immunoglobulin-like restricted axonal surface protein’; DM: protein is expressed in the dorsal funiculus and central midline of the spinal cord).^{63,64} Jaehrling *et al.* showed that reduced cell response, cell attachment, and neurite formation were observed, depending on the DM-GRASP density on the surface. DM-GRASP molecules on the gold nanoparticles do transinteract with DM-GRASP molecules in the plasma membrane of neurons, binding to spectrin, a heterotetramer in the cortical cytoskeleton. Particularly at a spacing of 70 nm a significantly reduced cellular response was observed that appeared to be independent from the overall relationship of neurite formation and particle density and could not be explained by reduced ligand density alone. Modeling the DM-GRASP-spectrin connection for different distances revealed that the formation of a stable spectrin network is hindered for 70 nm separation distance due to geometrical reasons. On substrates with 29, 54, and 86 nm spacings, each spectrin heterotetramer can be linked to three binding sites, while on 70 nm spaced patterns, only two binding sites of the spectrin heterotetramer to transinteracting DM-GRASP molecules are possible. This observation is another intriguing example how patterning of single proteins with nanometer resolution could translate into cellular response. Nanoparticle assemblies can also serve as templates for DNA nanostamping or protein nanoarrays with potential applications as biosensors. Stellacci and co-workers reported on a method where they used gold nanoparticles as a master for the production of DNA nanoarrays. This allowed them to take advantage of both the parallel fabrication technique and the nanoscale resolution of the micellar process.¹³⁰ Overall, the ability to pattern several square centimeter large arrays of functional proteins with user-defined resolutions down to the

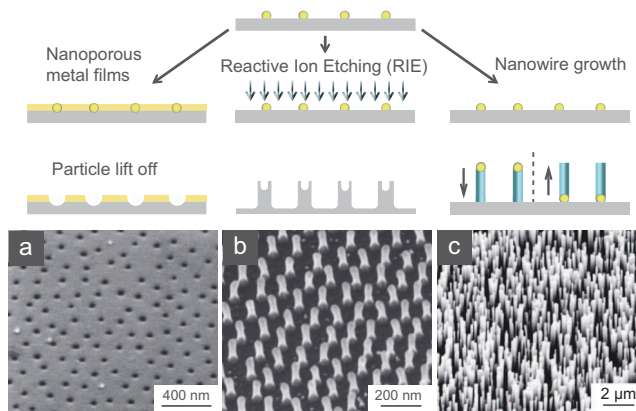


FIG. 11. (Color) Gold nanoparticles arrays can serve as a nanofabrication template for further sample processing. (a) Nanopore arrays are generated by using the particle array as a template for sputter deposition and subsequent removal of the nanoparticles. (b) Pillar arrays can be generated by using the nanoparticles as a masking material for reactive ion etching. (c) The particles are used as a seed for the growth of inorganic and organic materials directly on the particles. Adapted from Ref. 46.

single molecule level on a microscope glass slide makes BCMN a superior tool to study cell-surface or cell-cell interactions.^{50,53}

B. Materials science applications

Nanoparticle arrays are an excellent platform for functional material applications. The particles can, for example, serve as a mask for sputter deposition, as a resist for reactive ion etching (RIE), or as catalytically active seeds for nanowire growth. In the latter case, gold nanoparticles represent distinct anchor points for the deposition of inorganic and organic molecules. Examples for subsequent processing of nanoparticle templates are given in Fig. 11. Technological applications include templates for surface patterning,^{131,132} high-density data storage devices,^{133,134} quantum computers,¹³⁵ and optical materials such as photonic crystals⁶⁶ and antireflective coatings.^{136,137}

Nanoparticle arrays can be used as a shadow mask for the production of nanopore arrays. After the deposition of thin metal layers between the surface-bound nanoparticles, the particles are then removed by mechanical or chemical treatment, revealing a porous film. This is exemplarily shown for a TiO_x layer with 20 nm pores and a pore density greater than 10^9 pores/cm² [Fig. 11(a)]. The pore diameters reflect the original particle size. By controlling the nanopattern properties as described above, a wide variety of porous substrates with tunable pore size and density becomes accessible. Besides potential sensor applications,^{138,139} nanopore arrays can be used as template materials for the fabrication of nanowires^{140,141} and photonic structures.¹⁴²

Metallic nanoparticles can also be used as a mask for RIE of the supporting material. The success of this approach was demonstrated for the fabrication of semiconductor quantum structures.^{133,143} Gold nanoparticles were deposited on a quantum well surface (a GaAs or $\text{In}_{0.1}\text{Ga}_{0.9}\text{As}$ quantum well deposited on a GaAs wafer) fabricated with molecular beam

epitaxy. Using mild plasma conditions, dry etching of the sample resulted in an array of hexagonally ordered freestanding quantum wires with an aspect ratio of 1:10.

The use of controlled nanotopography for damping surface reflections also greatly improves the performance of functional optical materials. A fascinating example can be found in nature: compound eyes of specific moth and butterfly species are equipped with a periodic array of subwavelength-structured protuberances, which create an effective gradation of the refractive index between air and the cornea interface. Such a “moth eye structure” (MOES) reduces reflections from the surface of the chitin lens of insect eyes, while light transmission is increased at the same time. The significance of damping surface reflections becomes evident when considering that even glass transmits only about 92% of the incoming light due to reflection losses.

To fabricate artificial moth eye structures, a gold nanoparticle template is used as a mask for a reactive ion etching process. The etching rate of gold nanoparticles is slower than that of the glass substrate which results in a nanostructured surface. The spacing of the individual nanostructures resembles the spacing of the nanoparticle mask, making it easy to tune. Depending on process conditions and substrate, a variety of different nanostructures can be fabricated. On fused silica substrates pillarlike protrusions with a user-defined height between 90 and 180 nm can be created [Figs. 12(a) and 12(b)]. Altering the process also allows changing the shape of the nanostructures to a more conelike form with a fixed height of about 250 nm. Influencing the shape and height of these nanostructures significantly influences at which wavelength transmission is highest. Pillarlike moth eye structures cause an increase in transmission, especially in the UV range. Optimizing structure height for a wavelength of 248 nm increases transmission more than 6% compared to an unstructured sample [Fig. 12(e)]. Conelike structures, in comparison, are not as effective in the UV range due to a broader height distribution, which results in increased scattering at short wavelengths. Nevertheless, they are very effective at wavelengths starting from around 350 nm and have a broadband effect because of a less steep change of the refractive index. They increase transmission from the visible spectrum to the infrared, reaching a maximum of 99.8% between about 390 and 430 nm [Fig. 12(f)]. MOES fabrication with this technique is not limited to fused silica substrates. Other kinds of glasses, such as borosilicate glasses, can also be processed, resulting in conelike nanostructures [Fig. 12(c)].¹⁴⁴

Conventional antireflective coatings consist of thin films with a different refraction index than the substrate on which they are mounted. These coatings have several disadvantages which limit their functionality and usage: their performance depends on the angle of incidence and they are comparatively narrow banded. Furthermore, their temperature stability is limited as their coefficient of expansion is usually different from the substrate and the number of available materials with a suitable and stable index of refraction is, especially in the UV range, limited.¹⁴⁵ In contrast, moth eye

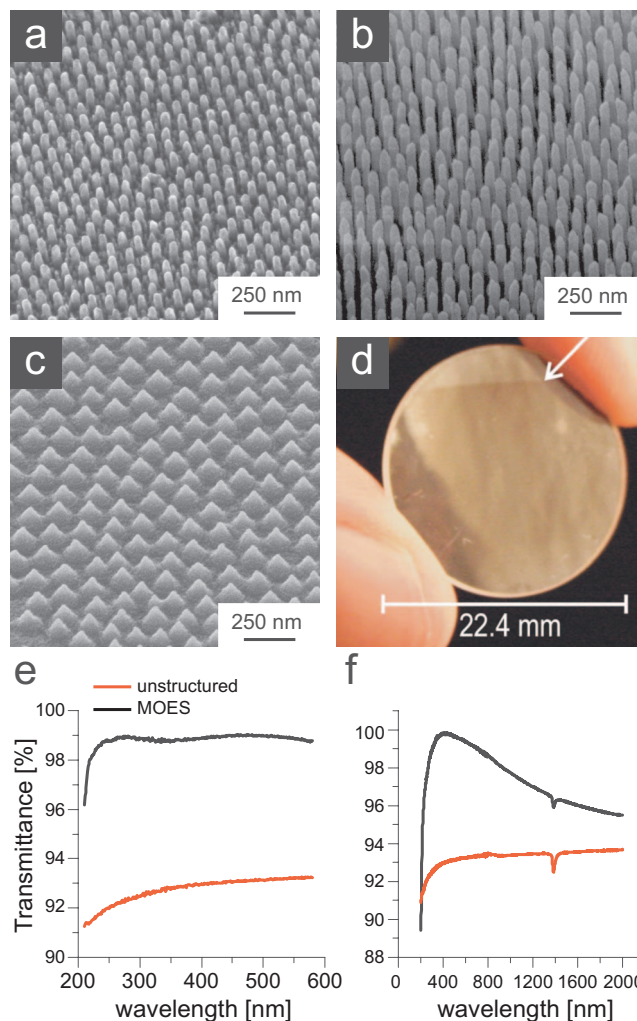


FIG. 12. (Color) (a)–(c) SE micrographs of different artificial moth eye structures (45° viewing angle). (a) and (b) Pillarlike structures on fused silica with a height of about (a) 90 nm and (b) approximately 180 nm. (c) Conelike structures, approximately 90 nm tall, fabricated on borosilicate glass. The spacing between the individual structures in (a)–(c) is about 85 nm. (d) This photograph of a processed lens demonstrates the antireflective effect. The transition between the structured (bottom) and unstructured (top) areas is indicated by the white arrow (picture adapted from Ref. 65). (e) and (f) Transmittance measurements of flat fused silica substrates decorated with moth eye structures on both sides compared to nonstructured samples. Pillarlike structures (e) show increased transmittance in the UV range whereas conelike structures with a height of about 250 nm (f) increase transmittance over a broad spectral range.

structures display none of these limitations. The possibility to fabricate moth eye structures on both plane and curved substrates like lenses [Fig. 12(d)] as well as the fact that it is a fast and cheap method to increase transmission and reduce reflection of light makes it the method of choice for improving the performance of functional devices such as projection optics or solar cells.¹⁴⁵

In addition to changing the optical properties of a material, nanopillar arrays can also reduce the coefficient of friction¹⁴⁶ and influence cell adhesion of human fibroblast cells.¹⁴⁷ Moreover, the topography of a surface has a significant impact on its wettability.¹⁴⁸ A difference of the contact angle of about 100° was observed between unstructured and

nanostructured samples, which corresponds to a substantial change of the surface properties from hydrophilic to hydrophobic without modification of the surface chemistry.¹⁴⁴ The water-repellent self-cleaning properties are solely a result of surface topology.

Particle templates may also be used as a catalytic seed for site-directed and controlled growth of inorganic^{46,149} and organic one-dimensional (1D) nanowires.^{67–69,149} Inorganic ZnO nanowires were grown by vapor-liquid-solid phase transport from nanoparticle templates consisting of gold clusters on a sapphire substrate.¹³³ Bulk Zn was heated up to temperatures higher than the Au-Zn eutectic point (between 500 and 900 °C) under argon flow. During the process Au clusters are saturated by the Zn vapor, leading to the formation of Au-Zn alloy nanodroplets. Further deposition of reactant molecules as a vapor, which adsorbs on to the liquid surface and diffuses into the droplet, leads to the epitaxial growth of ZnO nanoposts perpendicular to the substrate. The diameter of the nanowires is determined by the initial particle size. A similar approach was used to synthesize uniform silicon nanowires with a diameter of approximately 8 nm.⁹²

Highly notable is also the successful use of nanoparticle arrays as tools for templated growth of organic structures such as carbon nanotubes,^{92,93} 1D phthalocyanine nanowires,⁶⁸ and tubes^{45,68,69} with site-directed precision and controlled density. These materials have great potential as organic field-effect transistors or organic light emitting diodes. Interestingly, in the case of F₁₆CuPc wires, the size of the gold clusters was found to be critical for the growth. Single wires grew only on particles larger than 20 nm in diameter. The width of the F₁₆CuPc structure, however, was not influenced by the particle size.

IV. CONCLUSIONS

The ability to control surface patterning and structure formation on a nanoscopic length scale is a prerequisite for many applications in biomedical and materials science today and has become indispensable for future development in these fields. Over the past few years we have developed the concept of block copolymer micelle nanolithography as a versatile tool for nanoparticle synthesis and nanopatterning by pure self-assembly. The superiority of this method for the production of nanopatterns is based on several advantages: the ability to control the interparticle distance and the size of inorganic nanoparticles with nanoscopic accuracy and the possibility to influence processing rates. User-defined micro-nanopatterned interfaces can be created using a combination of micelle nanolithography and conventional top-down technology. In addition, these nanoparticle arrays can then be transferred to flexible substrates such as PEG-DA.

Due to its outstanding variability, this technique represents a powerful tool for numerous applications. Hexagonal arrays of gold particles may serve as anchor points for the selective binding of extracellular proteins, generating an artificial biological environment. Since the particles are transferable from inorganic to polymeric supports, this approach represents a valuable experimental platform to investigate

the activity of cells *in vivo* with precise control over relevant properties such as viscoelasticity, peptide composition, nanopography, and spatial organization.

Regarding materials science applications, metallic nanoparticles can be used as catalytic seeds for the deposition of inorganic and organic materials, for the growth of nanowire arrays, or as a masking material for thin film deposition. Furthermore, such nanoparticle arrays can serve as a mask for reactive ion etching, resulting in a nanostructured surface. Such surfaces show reduced friction coefficients, a change in wetting behavior as well as altered cell adhesion. Since the intervals between the nanostructures can be tuned to be smaller than the wavelength of the incident light, these structures have remarkable antireflective properties. Applied to optical functional materials this approach represents an inexpensive straightforward method for the fabrication of highly light-transmissive antireflective optical devices that can be used for display panels, projection optics, as well as heat-generating microscopic and excimer laser applications.

ACKNOWLEDGMENTS

Financial support by the Max Planck Society is highly appreciated. The work benefited greatly from structural suggestions and corrections provided by Nina Grunze.

- ¹R. P. Feynman, *Eng. Sci.* **23**, 22 (1960).
- ²R. F. W. Pease, *J. Vac. Sci. Technol. B* **10**, 278 (1992).
- ³Royal Society, "Nanoscience and Nanotechnologies: Opportunities and Uncertainties," *A Report by The Royal Society and The Royal Academy of Engineering*, London, July 2004.
- ⁴G. M. Whitesides, *Small* **1**, 172 (2005).
- ⁵D. Brambley, D. Martin, and P. D. Prewett, *Adv. Mater. Opt. Electron.* **4**, 55 (1994).
- ⁶W. M. Moreau, *Semiconductor Lithography: Principles and Materials* (Plenum, New York, 1988).
- ⁷M. Feldman and J. Sun, *J. Vac. Sci. Technol. B* **10**, 3173 (1992).
- ⁸J. P. Silverman, *J. Vac. Sci. Technol. B* **15**, 2117 (1997).
- ⁹R. Menon, A. Patel, D. Gil, and H. I. Smith, *Mater. Today* **8**, 26 (2005).
- ¹⁰S. Matsui, Y. Kojima, Y. Ochiai, and T. Honda, *J. Vac. Sci. Technol. B* **9**, 2622 (1991).
- ¹¹J. Melngailis, *J. Vac. Sci. Technol. B* **5**, 469 (1987).
- ¹²G. L. T. Chiu and J. M. Shaw, *IBM J. Res. Dev.* **41**, 3 (1997).
- ¹³S. J. Holmes, P. H. Mitchell, and M. C. Hakey, *IBM J. Res. Dev.* **41**, 7 (1997).
- ¹⁴K. J. Edler, *Philos. Trans. R. Soc. London, Ser. A* **362**, 2635 (2004).
- ¹⁵D. Philip and J. F. Stoddart, *Angew. Chem., Int. Ed. Engl.* **35**, 1155 (1996).
- ¹⁶G. M. Whitesides, *Nat. Biotechnol.* **21**, 1161 (2003).
- ¹⁷G. M. Whitesides and B. Grzybowski, *Science* **295**, 2418 (2002).
- ¹⁸B. D. Gates, Q. Xu, J. C. Love, D. B. Wolfe, and G. M. Whitesides, *Annu. Rev. Mater. Res.* **34**, 339 (2004).
- ¹⁹C. J. Love, L. A. Estroff, J. K. Kriebel, R. G. Nuzzo, and G. M. Whitesides, *Chem. Rev. (Washington, D.C.)* **105**, 1103 (2005).
- ²⁰A. Ulman, *Chem. Rev. (Washington, D.C.)* **96**, 1533 (1996).
- ²¹C. T. Black, R. Ruiz, G. Breyta, J. Y. Cheng, M. E. Colburn, K. W. Guarini, H.-C. Kim, and Y. Zhang, *IBM J. Res. Dev.* **51**, 605 (2007).
- ²²I. W. Hamley, *Nanotechnology* **14**, R39 (2003).
- ²³I. W. Hamley, *Angew. Chem., Int. Ed.* **42**, 1692 (2003).
- ²⁴C. Park, J. Yoon, and E. L. Thomas, *Polymer* **44**, 6725 (2003).
- ²⁵Y. Xia, B. Gates, Y. Yin, and Y. Lu, *Adv. Mater.* **12**, 693 (2000).
- ²⁶S. M. Yang, S. G. Jang, D. G. Choi, S. Kim, and H. K. Yu, *Small* **2**, 458 (2006).
- ²⁷Y. Xia, Y. Yin, Y. Lu, and J. McLellan, *Adv. Funct. Mater.* **13**, 907 (2003).
- ²⁸Y. Yin, Y. Lu, B. Gates, and Y. Xia, *J. Am. Chem. Soc.* **123**, 8718 (2001).
- ²⁹Y. Yin and Y. Xia, *Adv. Mater.* **13**, 267 (2001).

- ³⁰J. S. Ahn, P. T. Hammond, M. F. Rubner, and I. Lee, *Colloids Surf.*, **A** **259**, 45 (2005).
- ³¹P. T. Hammond, *Surface-Directed Colloid Patterning: Selective Deposition via Electrostatic and Secondary Interactions; in Colloids and Colloid Assemblies: Synthesis, Modification, Organization and Utilization of Colloid Particles*, edited by F. Caruso (Wiley-VCH Verlag GmbH & Co. KGaA, Weinheim, 2004).
- ³²G. M. Whitesides, E. Ostuni, S. Takayama, X. Jiang, and D. E. Ingber, *Annu. Rev. Biomed. Eng.* **3**, 335 (2001).
- ³³Y. Xia, J. A. Rogers, K. E. Paul, and G. M. Whitesides, *Chem. Rev.* (Washington, D.C.) **99**, 1823 (1999).
- ³⁴Y. Xia and G. M. Whitesides, *Angew. Chem.* **110**, 568 (1998).
- ³⁵R. D. Piner, J. Zhu, F. Xu, S. Hong, and C. A. Mirkin, *Science* **283**, 661 (1999).
- ³⁶K. Salaita, Y. Wang, and C. A. Mirkin, *Nat. Nanotechnol.* **2**, 145 (2007).
- ³⁷K. Wadu-Mesthrige, S. Xu, N. A. Amro, and G. Liu, *Langmuir* **15**, 8580 (1999).
- ³⁸S. Xu, S. Miller, P. E. Laibinis, and G. Liu, *Langmuir* **15**, 7244 (1999).
- ³⁹M. K. Herndon, R. T. Collins, R. E. Hollingsworth, P. R. Larson, and M. B. Johnson, *Appl. Phys. Lett.* **74**, 141 (1999).
- ⁴⁰L. J. Guo, *Adv. Mater.* **19**, 495 (2007).
- ⁴¹M. Arnold, E. A. Cavalcanti-Adam, R. Glass, J. Blümmel, W. Eck, M. Kantlehner, H. Kessler, and J. P. Spatz, *ChemPhysChem* **5**, 383 (2004).
- ⁴²R. Glass, M. Arnold, J. Blümmel, A. Küller, M. Möller, and J. P. Spatz, *Adv. Funct. Mater.* **13**, 569 (2003).
- ⁴³T. Lohmüller, E. Bock, and J. P. Spatz, *Adv. Mater.* **20**, 2297 (2008).
- ⁴⁴P. Liu and J. Ding, *Langmuir* **26**, 492 (2010).
- ⁴⁵T. Härtling, A. Seidenstücker, P. Olk, A. Plettl, P. Ziemann, and L. M. Eng, *Nanotechnology* **21**, 145309 (2010).
- ⁴⁶R. Glass, M. Arnold, E.-A. Cavalcanti-Adam, J. Blümmel, C. Haferkemper, C. Dodd, and J. P. Spatz, *New J. Phys.* **6**, 101 (2004).
- ⁴⁷B. Gorzolnik, P. Mela, and M. Möller, *Nanotechnology* **17**, 5027 (2006).
- ⁴⁸P. Mela, B. Gorzolnik, M. Bueckins, A. Mourran, J. Mayer, and M. Möller, *Small* **3**, 1368 (2007).
- ⁴⁹J. Chen, P. Mela, M. Möller, and M. Lensen, *ACS Nano* **3**, 1451 (2009).
- ⁵⁰D. Aydin, M. Schwieder, I. Louban, S. Knoppe, J. Ulmer, T. L. Haas, H. Walczak, and J. P. Spatz, *Small* **5**, 1014 (2009).
- ⁵¹D. Aydin *et al.*, *Langmuir* **26**, 14572 (2010).
- ⁵²S. V. Graeter, J. Huang, N. Perschmann, M. López-García, H. Kessler, J. Ding, and J. P. Spatz, *Nano Lett.* **7**, 1413 (2007).
- ⁵³T. Wolfram, F. Belz, T. Schoen, and J. P. Spatz, *BioInterphases* **2**, 44 (2007).
- ⁵⁴M. Arnold *et al.*, *Nano Lett.* **8**, 2063 (2008).
- ⁵⁵M. Arnold, M. Schwieder, J. Blümmel, E. A. Cavalcanti-Adam, M. López-García, H. Kessler, B. Geiger, and J. P. Spatz, *Soft Matter* **5**, 72 (2009).
- ⁵⁶E. A. Cavalcanti-Adam, A. Micoulet, J. Blümmel, J. Auernheimer, H. Kessler, and J. P. Spatz, *Eur. J. Cell Biol.* **85**, 219 (2006).
- ⁵⁷E. A. Cavalcanti-Adam, T. Volberg, A. Micoulet, H. Kessler, B. Geiger, and J. P. Spatz, *Biophys. J.* **92**, 2964 (2007).
- ⁵⁸C. Selhuber-Unkel, T. Erdmann, M. Lopez-Garcia, H. Kessler, U. S. Schwarz, and J. P. Spatz, *Biophys. J.* **98**, 543 (2010).
- ⁵⁹C. Selhuber-Unkel, M. Lopez-Garcia, H. Kessler, and J. P. Spatz, *Biophys. J.* **95**, 5424 (2008).
- ⁶⁰B. Geiger, J. P. Spatz, and A. D. Bershadsky, *Nat. Rev. Mol. Cell Biol.* **10**, 21 (2009).
- ⁶¹E. A. Cavalcanti-Adam, D. Aydin, V. C. Hirschfeld-Warneken, and J. P. Spatz, *HFSP J.* **2**, 276 (2008).
- ⁶²V. Hirschfeld-Warneken, M. Arnold, A. Cavalcanti-Adam, M. Lopez-García, H. Kessler, and J. Spatz, *Eur. J. Cell Biol.* **87**, 743 (2008).
- ⁶³S. Jaehrling, K. Thelen, T. Wolfram, and G. Pollerberg, *Nano Lett.* **9**, 4115 (2009).
- ⁶⁴K. Thelen, T. Wolfram, B. Maier, S. Jähring, A. Tinazli, J. Piehler, J. P. Spatz, and G. E. Pollerberg, *Soft Matter* **3**, 1486 (2007).
- ⁶⁵T. Lohmüller, M. Helgert, M. Sundermann, R. Brunner, and J. P. Spatz, *Nano Lett.* **8**, 1429 (2008).
- ⁶⁶M. R. Goncalves and O. Marti, *New J. Phys.* **5**, 160 (2003).
- ⁶⁷B. Mbenkum, E. Barrena, X. Zhang, M. Kelsch, and H. Dosch, *Nano Lett.* **6**, 2852 (2006).
- ⁶⁸E. Barrena, X. N. Zhang, B. N. Mbenkum, T. Lohmüller, T. N. Krauss, M. Kelsch, P. A. van Aken, J. P. Spatz, and H. Dosch, *ChemPhysChem* **9**, 1114 (2008).
- ⁶⁹T. N. Krauss, E. Barrena, T. Lohmüller, M. Kelsch, A. Breittling, P. A. van Aken, J. P. Spatz, and H. Dosch, *Chem. Mater.* **21**, 5010 (2009).
- ⁷⁰M. Park, C. Harrison, P. M. Chaikin, R. A. Register, and D. H. Adamson, *Science* **276**, 1401 (1997).
- ⁷¹R. Glass, M. Möller, and J. P. Spatz, *Nanotechnology* **14**, 1153 (2003).
- ⁷²J. P. Spatz, S. Mössmer, C. Hartmann, and M. Möller, *Langmuir* **16**, 407 (2000).
- ⁷³L. Leibler, *Macromolecules* **13**, 1602 (1980).
- ⁷⁴Z. Gao and A. Eisenberg, *Macromolecules* **26**, 7353 (1993).
- ⁷⁵J. Israelachvili, *Intramolecular and Surface Forces*, 2nd ed. (Academic Press, London, 1992).
- ⁷⁶J. Israelachvili, *Langmuir* **10**, 3774 (1994).
- ⁷⁷D. Izzo and C. M. Marques, *Macromolecules* **26**, 7189 (1993).
- ⁷⁸J. P. Spatz, A. Röscher, S. Sheiko, G. Krausch, and M. Möller, *Adv. Mater.* **7**, 731 (1995).
- ⁷⁹J. P. Spatz, S. Sheiko, and M. Möller, *Macromolecules* **29**, 3220 (1996).
- ⁸⁰J. P. Spatz, S. Mössmer, and M. Möller, *Chem.-Eur. J.* **2**, 1552 (1996).
- ⁸¹S. Mössmer, J. P. Spatz, M. Möller, T. Aberle, J. Schmidt, and W. Burckhard, *Macromolecules* **33**, 4791 (2000).
- ⁸²G. Kästle *et al.*, *Adv. Funct. Mater.* **13**, 853 (2003).
- ⁸³A. Ethirajan *et al.*, *Adv. Mater.* **19**, 406 (2007).
- ⁸⁴J. P. Wilcoxon and B. L. Abrams, *Chem. Soc. Rev.* **35**, 1162 (2006).
- ⁸⁵A. N. Shipway, E. Katz, and I. Willner, *ChemPhysChem* **1**, 18 (2000).
- ⁸⁶U. V. M. Kreibitz, *Optical Properties of Metal Clusters* (Springer, Heidelberg, 1995).
- ⁸⁷C. Langhammer, Z. Yuan, I. Zoric, and B. Kasemo, *Nano Lett.* **6**, 833 (2006).
- ⁸⁸S. Link and M. A. El-Sayed, *Annu. Rev. Phys. Chem.* **54**, 331 (2003).
- ⁸⁹P. Mulvaney, *Langmuir* **12**, 788 (1996).
- ⁹⁰M. Schnippering, M. Carrara, A. Foelske, R. Kötz, and D. J. Fermín, *Phys. Chem. Chem. Phys.* **9**, 725 (2007).
- ⁹¹J. Sharma, J. P. Vivek, and K. P. Vijayamohan, *J. Nanosci. Nanotechnol.* **6**, 3464 (2006).
- ⁹²J. Lu, S. S. Yi, T. Kopley, C. Qian, J. Liu, and G. Erdogan, *J. Phys. Chem. B* **110**, 6655 (2006).
- ⁹³D. Takagi, Y. Homma, H. Hibino, S. Suzuki, and Y. Kobayashi, *Nano Lett.* **6**, 2642 (2006).
- ⁹⁴P. Hanarp, M. Kaelell, and D. S. Sutherland, *J. Phys. Chem. B* **107**, 5768 (2003).
- ⁹⁵K. L. Kelly, E. Coronado, L. L. Zhao, and G. C. Schatz, *J. Phys. Chem. B* **107**, 668 (2003).
- ⁹⁶L. M. Liz-Marzán, *Langmuir* **22**, 32 (2006).
- ⁹⁷W. Rechberger, A. Hohenau, A. Leitner, J. R. Krenn, B. Lamprecht, and F. R. Aussenegg, *Opt. Commun.* **220**, 137 (2003).
- ⁹⁸N. Walter, C. Selhuber, H. Kessler, and J. P. Spatz, *Nano Lett.* **6**, 398 (2006).
- ⁹⁹S. Krishnamoorthy, P. Raphaël, J. Brugger, H. Heinzelmann, and C. Hinderling, *Adv. Funct. Mater.* **16**, 1469 (2006).
- ¹⁰⁰J. Bansmann, S. Kielbassa, H. Hoster, F. Weigl, H. G. Boyen, U. Wiedwald, P. Ziemann, and R. J. Behm, *Langmuir* **23**, 10150 (2007).
- ¹⁰¹M. Möller, C. S. Hartmann, J. Sihler, S. Fricker, V. Z. H. Chan, and J. P. Spatz, *Polym. Mater. Sci. Eng.* **90**, 255 (2004).
- ¹⁰²S. Förster and T. Plantenberg, *Angew. Chem., Int. Ed.* **41**, 688 (2002).
- ¹⁰³M. Arnold, Dissertation, University of Heidelberg, 2005.
- ¹⁰⁴A. A. Darhuber, S. M. Troian, S. M. Miller, and S. Wagner, *J. Appl. Phys.* **87**, 7768 (2000).
- ¹⁰⁵K. R. Brown and M. J. Natan, *Langmuir* **14**, 726 (1998).
- ¹⁰⁶J. Turkevich, P. C. Stevenson, and J. Hillier, *Discuss. Faraday Soc.* **11**, 55 (1951).
- ¹⁰⁷G. Stremmsdoerfer, J. R. Martin, and P. Clechet, *Proc.-Electrochem. Soc.* **92-93**, 305 (1992).
- ¹⁰⁸J. P. Spatz, *Angew. Chem., Int. Ed.* **41**, 3359 (2002).
- ¹⁰⁹S. H. Yun, B. H. Sohn, J. C. Jung, W. C. Zin, M. Ree, and J. W. Park, *Nanotechnology* **17**, 450 (2006).
- ¹¹⁰J. P. Spatz, V. Z. H. Chan, S. Mößmer, F.-M. Kamm, A. Plettl, P. Ziemann, and M. Möller, *Adv. Mater.* **14**, 1827 (2002).
- ¹¹¹M. M. Stevens and J. H. George, *Science* **310**, 1135 (2005).
- ¹¹²C. A. Mirkin and C. M. Niemeyer, *Nanobiotechnology II: More Concepts and Applications* (Wiley-VCH, New York, 2007).
- ¹¹³C. M. Niemeyer and C. A. Mirkin, *Nanobiotechnology: Concepts, Applications and Perspectives* (Wiley-VCH, New York, 2004).
- ¹¹⁴I. Willner, R. Baron, and B. Willner, *Biosens. Bioelectron.* **22**, 1841 (2007).
- ¹¹⁵K.-B. Lee, S.-J. Park, C. A. Mirkin, J. C. Smith, and M. Mrksich, *Science*

- 295, 1702 (2002).
- ¹¹⁶M. van den Heuvel and C. Dekker, *Science* **317**, 333 (2007).
- ¹¹⁷S. Howorka, S. Cheley, and H. Bayley, *Nat. Biotechnol.* **19**, 636 (2001).
- ¹¹⁸C. R. Martin and P. Kohli, *Nat. Rev. Drug Discovery* **2**, 29 (2003).
- ¹¹⁹L. M. Adleman, *Science* **266**, 1021 (1994).
- ¹²⁰M. A. Firestone, M. L. Shank, S. G. Sligar, and P. W. Bohn, *J. Am. Chem. Soc.* **118**, 9033 (1996).
- ¹²¹J. Groll, K. Albrecht, P. Gasteier, S. Riethmüller, U. Ziener, and M. Möller, *ChemBioChem* **6**, 1782 (2005).
- ¹²²J. Blümmel, N. Perschmann, D. Aydin, J. Drinjakovic, T. Surrey, M. Lopez-Garcia, H. Kessler, and J. P. Spatz, *Biomaterials* **28**, 4739 (2007).
- ¹²³G. Kenaousis, J. Voros, D. Elbert, N. Huang, R. Hofer, L. Ruiz-Taylor, M. Textor, J. A. Hubbell, and N. D. Spencer, *J. Phys. Chem. B* **104**, 3298 (2000).
- ¹²⁴R. O. Hynes, *Cell* **48**, 549 (1987).
- ¹²⁵E. Ruoslahti, *Annu. Rev. Cell Dev. Biol.* **12**, 697 (1996).
- ¹²⁶L. Y. Koo, D. J. Irvine, A. M. Mayes, D. A. Lauffenburger, and L. G. Griffith, *J. Cell. Sci.* **115**, 1423 (2002).
- ¹²⁷G. Maheshwari, G. Brown, D. A. Lauffenburger, A. Wells, and L. G. Griffith, *J. Cell. Sci.* **113**, 1677 (2000).
- ¹²⁸S. P. Massia and J. A. Hubbell, *J. Cell Biol.* **114**, 1089 (1991).
- ¹²⁹J. P. Spatz and B. Geiger, *Methods Cell Biol.* **83**, 89 (2007).
- ¹³⁰O. Akbulut, J. M. Jung, R. D. Bennett, Y. Hu, H.-T. Jung, R. E. Cohen, A. M. Mayes, and F. Stellacci, *Nano Lett.* **7**, 3493 (2007).
- ¹³¹L. Cao, J. A. Massey, M. A. Winnik, I. Manners, S. Riethmüller, F. Banhart, J. P. Spatz, and M. Möller, *Adv. Funct. Mater.* **13**, 271 (2003).
- ¹³²J. P. Spatz, P. Eibeck, S. Mössmer, M. Möller, T. Herzog, and P. Ziemann, *Adv. Mater.* **10**, 849 (1998).
- ¹³³M. Haupt, S. Miller, R. Glass, M. Arnold, R. Sauer, K. Thonke, M. Möller, and J. P. Spatz, *Adv. Mater.* **15**, 829 (2003).
- ¹³⁴K. Shin, K. A. Leach, J. T. Goldbach, D. H. Kim, J. Y. Jho, M. Tuominen, C. J. Hawker, and T. P. Russell, *Nano Lett.* **2**, 933 (2002).
- ¹³⁵D. P. DiVincenzo, *Science* **270**, 255 (1995).
- ¹³⁶M. Ibn-Elhaj and M. Schadt, *Nature (London)* **410**, 796 (2001).
- ¹³⁷S. Walheim, E. Schaeffer, J. Mlynek, and U. Steiner, *Science* **283**, 520 (1999).
- ¹³⁸S. Ahl, P. J. Cameron, J. Liu, W. Knoll, J. Erlebacher, and F. Yu, *Plasmonics* **3**, 13 (2008).
- ¹³⁹T. Lohmüller *et al.*, *J. Micromech. Microeng.* **18**, 115011 (2008).
- ¹⁴⁰G. Sauer, G. Brehm, S. Schneider, K. Nielsch, R. B. Wehrspohn, J. Choi, H. Hofmeister, and U. Gösele, *J. Appl. Phys.* **91**, 3243 (2002).
- ¹⁴¹M. Steinhart, J. Wendorff, A. Greiner, R. B. Wehrspohn, K. Nielsch, J. Schilling, J. Choi, and U. Gösele, *Science* **296**, 1997 (2002).
- ¹⁴²A. Birner, R. Wehrspohn, U. Gösele, and K. Busch, *Adv. Mater.* **13**, 377 (2001).
- ¹⁴³M. Haupt, S. Miller, A. Ladenburger, R. Sauer, K. Thonke, J. P. Spatz, S. Riethmüller, M. Möller, and F. Banhart, *J. Appl. Phys.* **91**, 6057 (2002).
- ¹⁴⁴T. Lohmüller, R. Brunner, and J. P. Spatz, *Improved Properties of Optical Surfaces by Following the Example of the Moth Eye* (INTECH, Croatia, 2010).
- ¹⁴⁵E. Yoon, R. Singh, H. Kong, B. Kim, D.-H. Kim, H. E. Jeong, and K. Y. Suh, *Tribol. Lett.* **21**, 31 (2006).
- ¹⁴⁶C. H. Choi, S. Heydarkhan-Hagvall, B. M. Wu, J. C. Dunn, R. E. Beygui, and C. J. Kim, *J. Biomed. Mater. Res. Part A* **89A**, 804 (2009).
- ¹⁴⁷C.-H. Choi, S. Heydarkhan-Hagvall, B. M. Wu, J. C. Y. Dunn, R. E. Beygui, and C.-J. Kim, *J. Biomed. Mat. Res., A* **89**, 804 (2008).
- ¹⁴⁸T. Lohmüller, Dissertation, University of Heidelberg, 2008.
- ¹⁴⁹B. N. Mbenkum, A. S. Schneider, G. Schütz, C. Xu, G. Richter, P. A. van Aken, G. Majer, and J. P. Spatz, *ACS Nano* **4**, 1805 (2010).